Morris, J.D., Villinger, H.W., and Klaus, A. (Eds.)
Proceedings of the Ocean Drilling Program, Scientific Results Volume 205

10. Data Report: Permeability and Consolidation Properties of Subducting Sediments off Costa Rica, ODP Leg 205[1]

Alexander W. McKiernan[2] and Demian M. Saffer[2]

ABSTRACT

Vertical permeability and sediment consolidation measurements were taken on seven whole-round drill cores from Sites 1253 (three samples), 1254 (one sample), and 1255 (three samples) drilled during Ocean Drilling Program Leg 205 in the Middle America Trench off of Costa Rica's Pacific Coast. Consolidation behavior including slopes of elastic rebound and virgin compression curves (C_c) was measured by constant rate of strain tests. Permeabilities were determined from flow-through experiments during stepped-load tests and by using coefficient of consolidation (C_v) values continuously while loading. Consolidation curves and the Casagrande method were used to determine maximum preconsolidation stress. Elastic slopes of consolidation curves ranged from 0.097 to 0.158 in pelagic sediments and 0.0075 to 0.018 in hemipelagic sediments. C_c values ranged from 1.225 to 1.427 for pelagic carbonates and 0.504 to 0.826 for hemipelagic clay-rich sediments. In samples consolidated to an axial stress of ~20 MPa, permeabilities determined by flow-through experiments ranged from a low value of 7.66×10^{-20} m^2 in hemipelagic sediments to a maximum value of 1.03×10^{-16} m^2 in pelagic sediments. Permeabilities calculated from C_v values in the hemipelagic sediments ranged from 4.81×10^{-16} to 7.66×10^{-20} m^2 for porosities 49.9%–26.1%.

[1]McKiernan, A.W., and Saffer, D.M., 2006. Data report: Permeability and consolidation properties of subducting sediments off Costa Rica, ODP Leg 205. *In* Morris, J.D., Villinger, H.W., and Klaus, A. (Eds.), *Proc. ODP, Sci. Results,* 205, 1–24 [Online]. Available from World Wide Web: <http://www-odp.tamu.edu/publications/205_SR/VOLUME/CHAPTERS/203.PDF>. [Cited YYYY-MM-DD]
[2]Pennsylvania State University, 320 Deike Building, University Park PA 16802, USA. Correspondence author: **amckiern@geosc.psu.edu**

Initial receipt: 22 June 2004
Acceptance: 24 May 2005
Web publication: 20 January 2006
Ms 205SR-203

INTRODUCTION

During September and October 2002, Ocean Drilling Program (ODP) Leg 205 visited the Middle America Trench off the Nicoya Peninsula, Costa Rica. Sites 1253, 1254, and 1255 (Fig. F1) were drilled along a transect trending roughly northeast-southwest across the deformation front associated with subduction of the Cocos plate beneath the Caribbean plate. Site 1253 is located 0.2 km seaward, Site 1254 1.5 km arcward, and Site 1255 0.4 km arcward of the deformation front (Fig. F1). The ~380-m-thick incoming sedimentary section is completely underthrust beneath a margin wedge and is composed of ~200 m of pelagic carbonates overlain by ~180 m of hemipelagic claystone (Fig. F1B) (e.g., Morris, Villinger, Klaus, et al., 2003). Samples from Site 1253 used in this study are calcareous mudstones from near the base of the incoming sedimentary section, between 380.07 and 394.91 meters below seafloor (mbsf) (Table T1). The single sample from Site 1254 is from near the décollement base at 366.74 mbsf (Table T1). Samples from Site 1255 are from underthrust sediments at depths of 134.89–152.38 mbsf (Table T1). Samples from Sites 1254 and 1255 are composed of hemipelagic mudstones. Exact sample location data are given in Table T1.

F1. Bathymetric map and seismic line, p. 7.

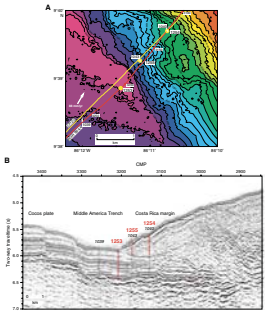

T1. Sample locations, p. 13.

METHODS

Consolidation and permeability data were collected simultaneously from ODP drill cores using a fixed-ring uniaxial consolidation cell produced by GDS Instruments (Tritech 50 kN). This cell, in combination with fluid pressure controllers also produced by GDS Instruments (Fig. F2), allows monitoring and manipulation of fluid pressure at the base and top of the cell during consolidation tests. Experimental equipment was controlled via computer, and all data, including axial displacement (±1 mm precision), axial stress (±0.1 kPa), backpressures (±1 kPa), base pressure (±0.1 kPa), and back and base volumes (±1 mL), were logged digitally in real time.

F2. Uniaxial consolidation system, p. 8.

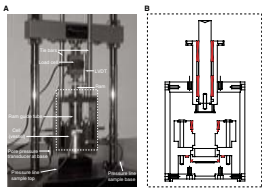

Drill core samples collected during Leg 205 were enclosed in plastic wrap and stored in ODP core liners sealed at both ends with hard plastic caps, electrical tape, and wax to prevent dehydration. On shore, samples were stored in these containers at 4°C and 100% humidity until immediately before being trimmed and placed into the consolidation cell. Samples were cut into cylinders 2 cm × 5 cm and fit into the ring for placement in the consolidation cell. Filter paper was placed on top and bottom of the sample, and the ring was placed into the cell with centered hastalloy porous discs between the sample and fluid inlets on top and bottom. In general, all experimental procedures followed American Society for Testing and Materials (ASTM) guidelines for uniaxial consolidation (ASTM, 1996, 1998). Excess cuttings were weighed, dried at 105°C for 24 hr, and reweighed to determine initial porosity.

Distilled deaerated water was used for all experiments. Water was deaerated using the Nold DeAerator, which lowers dissolved oxygen content to <10 ppb. Once in the consolidation cell, fluid backpressure was slowly raised over a period of 24 hr to between 300 and 500 kPa to ensure sample saturation and help evacuate and/or force any included gas into solution.

F3. Consolidation results, p. 9.

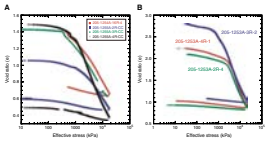

Samples were consolidated through constant rate of strain (CRS) tests (Fig. F3). In these tests, strain rate was maintained by a computer-controlled load frame using a steel ram. The sample top was kept open

to controlled backpressure (300 kPa), and the port at the sample base was kept closed. The resulting stress, basal pore pressure, and axial displacement were recorded continuously at the precision noted above. CRS tests allow for continuous data collection during compression, which helps to define a complete stress-strain curve. Maximum preconsolidation stress (P_c') estimates for samples from Site 1253 were obtained using the Casagrande method (von Fay, 1986). Stress-strain curves for samples from Sites 1254 and 1255 were of such low quality that the Casagrande construction could not be used reliably; instead P_c' values for these samples were obtained by noting the extrapolated intersection of the virgin and elastic portions of the stress-strain curve. Estimates of in situ porosity given in Table T2 are based on the intersection of the given sample's consolidation curve with the line $\sigma' = P_c'$, and in situ permeabilities were calculated using the in situ porosity estimate and a laboratory-derived relationship between log permeability and porosity for each sample.

T2. Sample permeability and consolidation data, p. 14.

If overpressures developed during laboratory consolidation, CRS tests also allowed for calculation of coefficient of consolidation (C_v), from which permeabilities throughout consolidation could be obtained (ASTM, 1998). Sample void ratios during testing were calculated based on axial displacements and initial void ratios. Average effective axial stress (σ'_v) across the sample was calculated based on measured axial load and basal excess fluid pressure (ASTM, 1998):

$$\sigma'_v = (\sigma_v^3 - 2\,\sigma_v^2 u_b + \sigma_v u_b^2)^{1/3},$$

where

σ_v = applied effective stress at sample top, and
u_b = excess fluid pressure at sample base.

In general, samples were consolidated to ~20 MPa axial stress. An effort was made to consolidate samples at a rate that would create excess pore pressure between 3% and 30% of effective axial load, which is ideal for permeability calculations using C_v values (ASTM, 1998). Hydraulic conductivities (K), were calculated using values of C_v by

$$C_v \times M_v \times \gamma_w = K$$

where

$$C_v = -[H^2 \times \log(\sigma_{v2}/\sigma_{v1})]/\{2 \times \Delta t \times \log[1 - (u_b/\sigma_v)]\},$$

$$M_v = (1/H_1) \times (H_1 - H_2)/(\sigma_{v2}' - \sigma_{v1}')$$

and

H = sample height,
σ_{v1} = applied axial load – backpressure at t_1,
σ_{v2} = applied axial load – backpressure at t_2,
Δt = $t_2 - t_1$,
u_b = average excess fluid pressure at the base between t_2 and t_1,
σ_v = average applied axial load – backpressure between t_2 and t_1,
σ_v' = effective stress (as defined above),
γ_w = unit weight of water = 9810 N, and

M_v = volumetric compressibility (Pa^{-1}).

Flow-through permeability tests were conducted at the completion of CRS testing for comparison with permeabilities calculated from C_v values or, where no overpressures developed to determine C_v (all Site 1253 samples), to gather permeability data. Flow-through permeability tests were also conducted on a second sample from each whole-round core where available and where core quality permitted to provide independent measurements of sample permeabilities for comparison with those determined from C_v values.

For these tests, we prepared samples as for CRS tests but conducted stepped loading using a stress multiplier of 1.5 or 2. A series of flow-through experiments were conducted after each consolidation stage. In flow-through tests, fluid was pumped into the top of the sample at a constant rate while constant pressure was maintained at the cell base. Pressure at the top of the cell was monitored to determine the pressure difference (d*P*) across the sample for each flow rate (Fig. **F4A, F4B**). In flow-through tests, the pressure gradient was not allowed to exceed 10% of the axial load and, in most cases, was <5% of effective stress at the sample top. Values of d*P* were then converted to head by

$$dh = dP/(\gamma_w \times g),$$

where

d*P* = pressure difference across sample (Pa),
g = gravitational constant (9.81 m/s²), and
γ_w = unit weight of water (9810 N).

By Darcy's Law, *K* is defined by the proportionality between specific discharge (*Q*/A) and head gradient (d*h*/d*l*):

$$Q/A = -K \times (dh/dl),$$

where

Q = fluid flux (m^3/s),
A = sample area (constant at 0.002 m^2),
d*h* = head difference across sample (m), and
d*l* = path length of flow (equal to sample height, m).

In flow-through tests, varying *Q* produces different d*P* values (Fig. **F4**). Standard deviations of "equilibrium" d*P* values were calculated to constrain error for each determination of d*P*. Errors in d*P* are generally <5% but reach a maximum of 22% at flow rates near the minimum capability of the flow pump due to nonconstant introduction of water at the sample top. For each permeability reported, flow-through tests were conducted across the same path length, d*l* (porosity is constant); pressure differences are thus proportional only to *Q*. After plotting d*h*/d*l* vs. *Q*/A for each flow rate ($3 \le n \le 5$), *K*-values were obtained by calculating the slope of a least-squares best-fit line to the data and using the origin as an additional data point (zero pressure difference with zero flow). Minimum and maximum values of *K* were obtained by calculating least-squares fits to high and low errors for d*h*/d*l*, producing lines with slopes equal to K_{min} and K_{max} (Fig. **F4C, F4D**).

F4. Flow-through permeability data, p. 10.

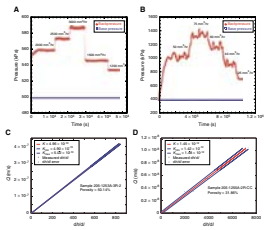

All hydraulic conductivities were converted to permeability, k, by:

$$k = (K \times \mu)/(p \times g)$$

where

μ = viscosity of water (0.001002 Pa·s),
p = density of water (1000 kg/m^3), and
g = gravitational constant (9.81 m/s^2).

RESULTS

The elastic slopes of consolidation curves ranged from 0.097 to 0.158 in pelagic sediments, and 0.0075 to 0.018 in hemipelagic sediments. Values of C_c ranged from 1.225 to 0.427 in pelagic carbonates and 0.504 to 0.826 in hemipelagic sediments (Table T2; Fig. F3).

Permeabilities calculated from C_v values in the hemipelagic sediments range from 7.66×10^{-20} to 4.81×10^{-16} m^2 over a porosity range of 49.9%–26.1% and follow linear relationships relating log(k) to porosity for each sample (Table T3, T4; Fig. F5). Permeability varies by about an order of magnitude between samples at a given porosity. Permeabilities determined from flow-through experiments on the hemipelagic sediments ranged from 4.81×10^{-16} to 7.66×10^{-20} m^2 over a porosity range of 49.9%–26.1% (Table T5, T6, Fig. F6); these values are consistent with permeabilities determined from C_v values. Permeabilities of pelagic sediments determined by flow-through experiments ranged from 5.07×10^{-17} to 1.03×10^{-16} m^2 over a range of porosity of 45.8%–50.1% (Table T5, T6; Fig. F6).

ACKNOWLEDGMENTS

This research used samples and/or data provided by the Ocean Drilling Program (ODP). ODP is sponsored by the U.S. National Science Foundation (NSF) and participating countries under management of Joint Oceanographic Institutions (JOI), Inc. D.M. Saffer was supported by NSF grant OCD-0241482 and a JOI-United States Science Advisory Committee (USSAC) grant. We thank the captain and crew of the *JOIDES Resolution*, without whom this research would have been impossible. We thank Achim Kopf and Henrich Villinger for their constructive comments and Lorri Peters for editorial comments.

T3. Flow-through permeability results and error, p. 15.

T4. Flow-through test data, p. 18.

F5. Hemipelagic permeabilities, p. 11.

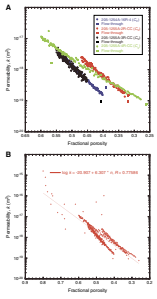

T5. Permeability equations, p. 17.

T6. C_v, M_v, and K values, p. 16.

F6. Flow-through permeability determinations, p. 12.

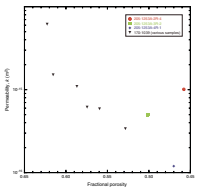

REFERENCES

ASTM International, 1996. Standard test method for one-dimensional consolidation properties of soils (Standard D2435–96). In *Annual Book of ASTM Standards* (Vol. 04.08): Philadelphia (Am. Soc. Testing and Mater.).

ASTM International, 1998. Standard test method for one-dimensional consolidation properties of soils using controlled-strain loading (Standard D4186–89). In *Annual Book of ASTM Standards* (Vol. 04.08): Philadelphia (Am. Soc. Testing and Mater.)

Morris, J.D., Villinger, H.W., Klaus, A., 2003. *Proc. ODP, Init. Repts.,* 205 [Online]. Available from World Wide Web: <http://www-odp.tamu.edu/publications/205_IR/205ir.htm>. [Cited 2004-06-01]

Saffer, D.M., Silver, E.A., Fisher, A.T., Tobin, H., and Moran, K., 2000. Inferred pore pressures at the Costa Rica subduction zone: implications for dewatering processes. *Earth Planet. Sci. Lett.,* 177:193–207.

von Fay, K.F., Byers, J.G., and Kunzer, B.A., 1986. Desktop computer application for consolidation testing and analysis. *In* Yong, R.N., and Townsend, F.C. (Eds.), *Consolidation of Soils: Testing and Evaluation:* Philadelphia (Am. Soc. Testing and Mater.), 217–235.

Figure F1. A. Bathymetric map of Leg 205 and 170 transects with borehole locations. **B.** Seismic line showing Leg 170 drill Sites 1039, 1040, and 1043 and Leg 205 drill Sites 1253, 1254, and 1255 adapted from Morris, Villinger, Klaus, et al., 2003. CMP = common midpoint.

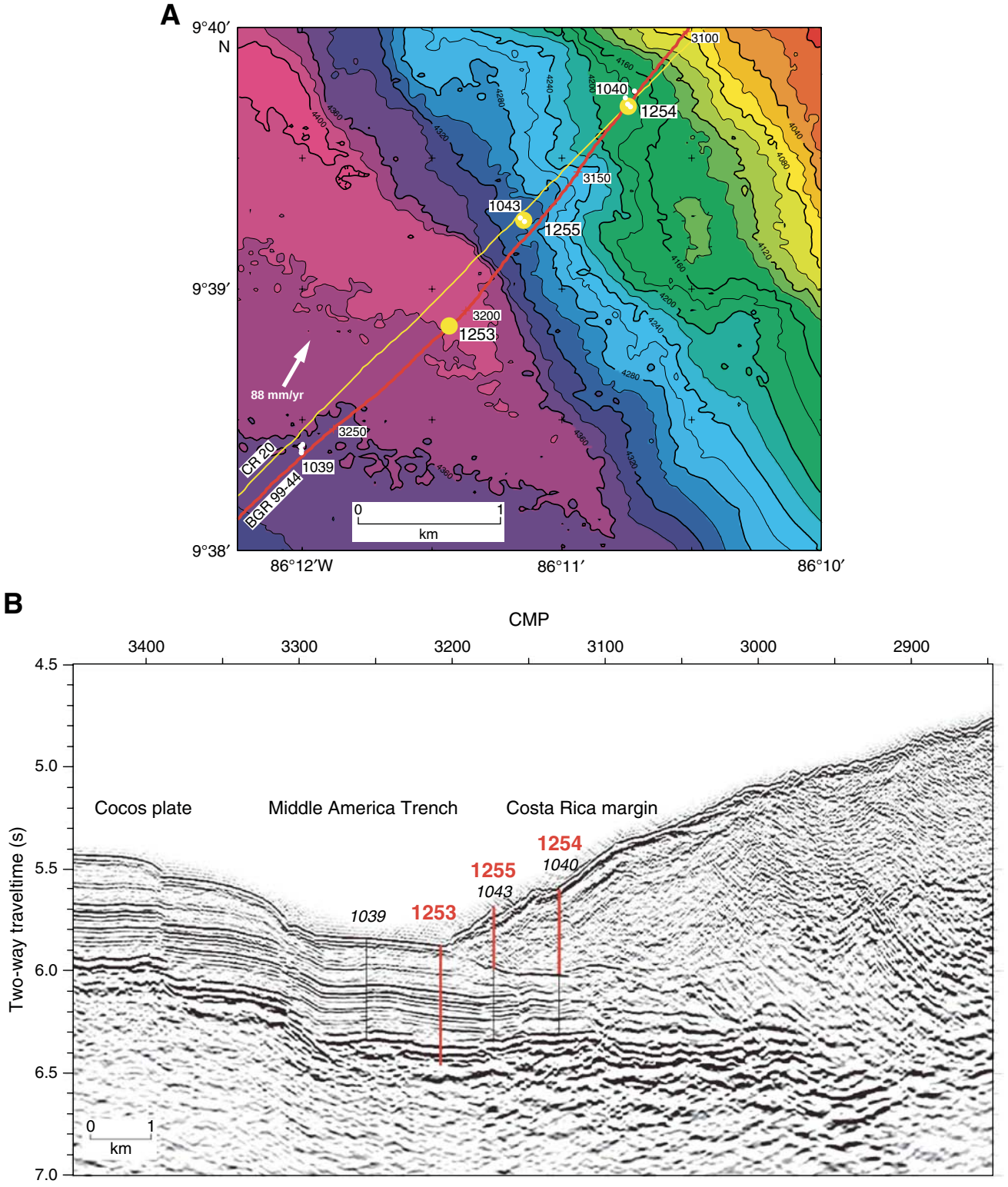

Figure F2. (**A**) Annotated photograph and (**B**) scaled and enlarged blueprint of uniaxial consolidation system (blueprint encompasses area outlined by white dashed line in photo). X = O-ring seals. LVDT = Linear Variable Displacement Transducer.

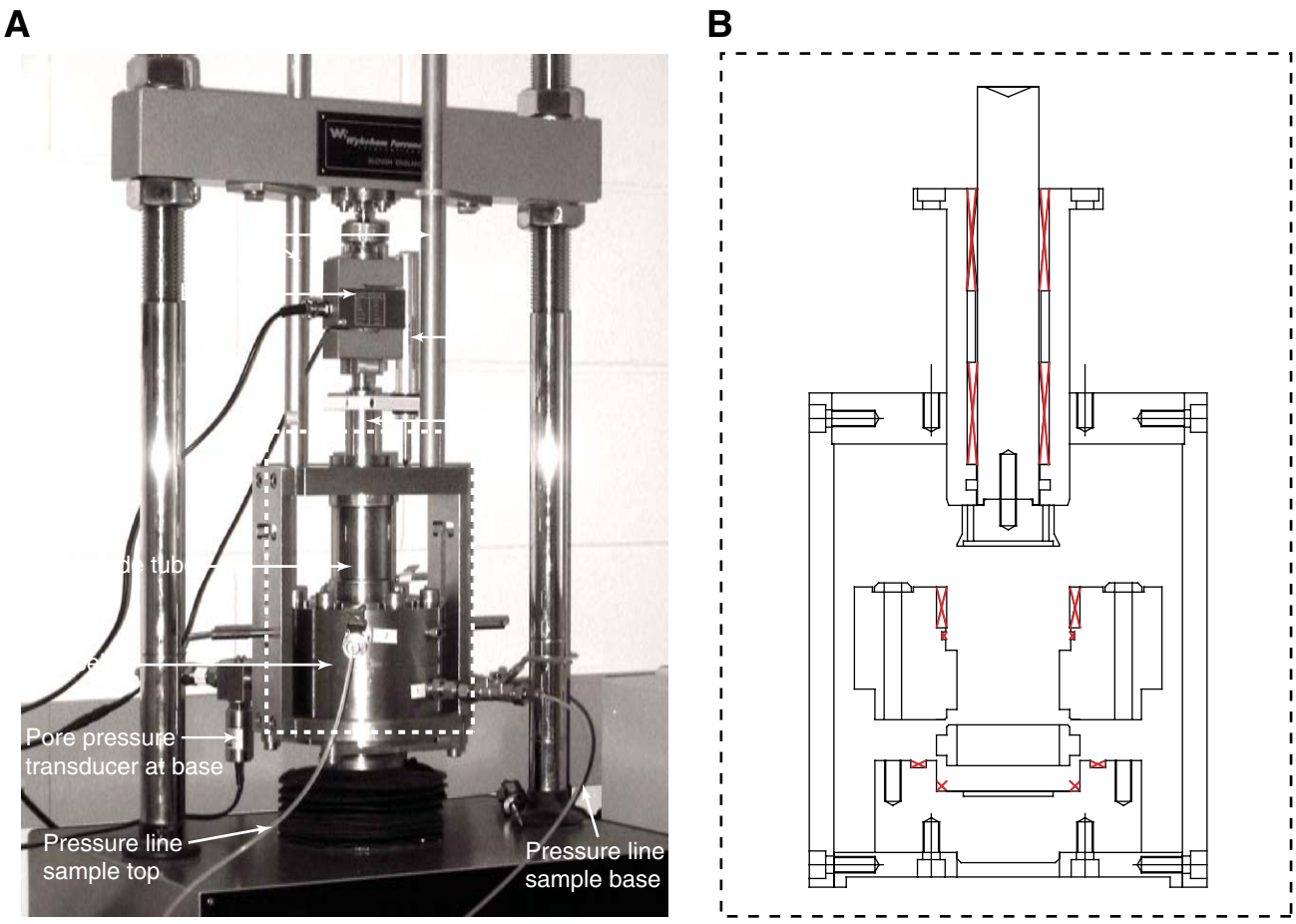

Figure F3. Consolidation results (stress-strain curves) including unloading where available. Slopes of virgin compression curves (C_c), elastic recompression/unloading curves, and values of P_c' are determined from these data. **A.** Results for hemipelagic samples from Sites 1254 and 1255. **B.** Results for pelagic samples from Site 1253.

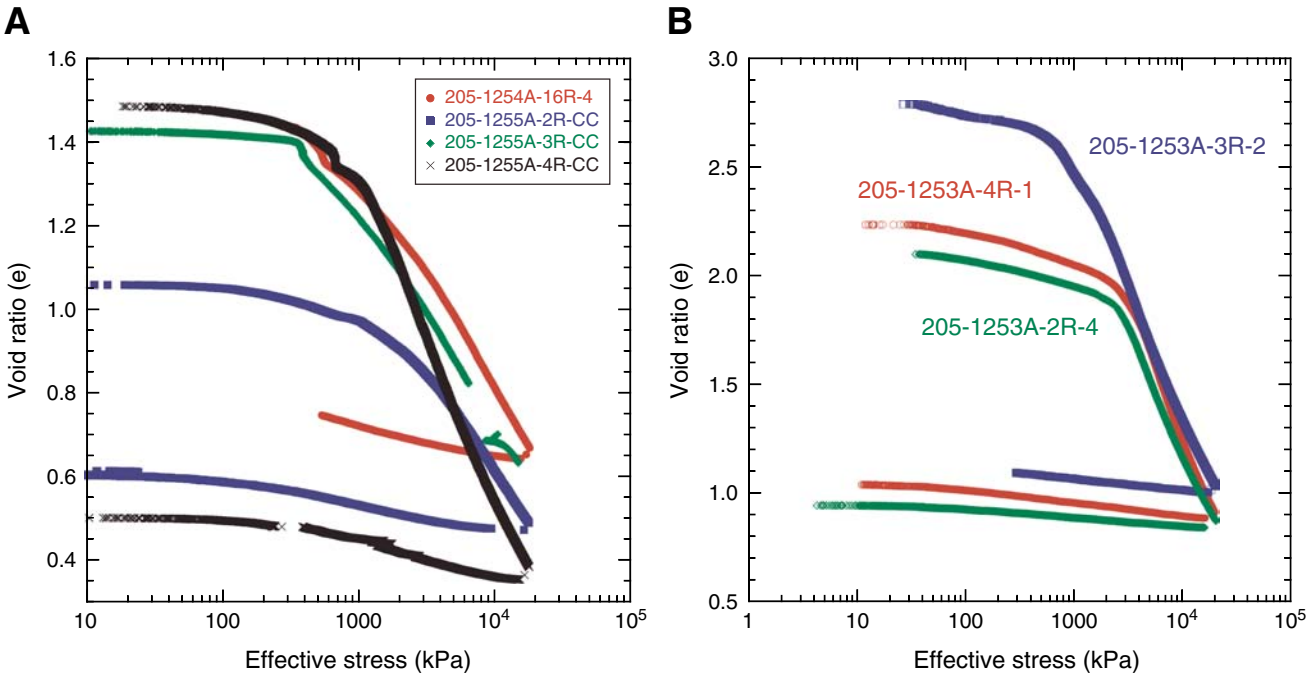

Figure F4. Flow-through permeability data and examples of best-fit lines to Q/A vs. dh/dl. **A.** Section 205-1253A-3R-2 dP vs. time for five flow rates as annotated. These data are typical for the pelagic samples. **B.** Sample 205-1255A-2R-CC dP vs. time. This example illustrates the significant variability in dP observed at low permeabilities (high effective stresses), owing to low flow rates, near the lower limit of pump capability. These data are typical of the lowest permeabilities measured (low porosity, high effective stress). **C.** Best-fit lines for K, K_{min}, and K_{max} for Section 205-1253A-3R-2. **D.** Best-fit lines for K, K_{min}, and K_{max} for Sample 205-1255A-2R-CC.

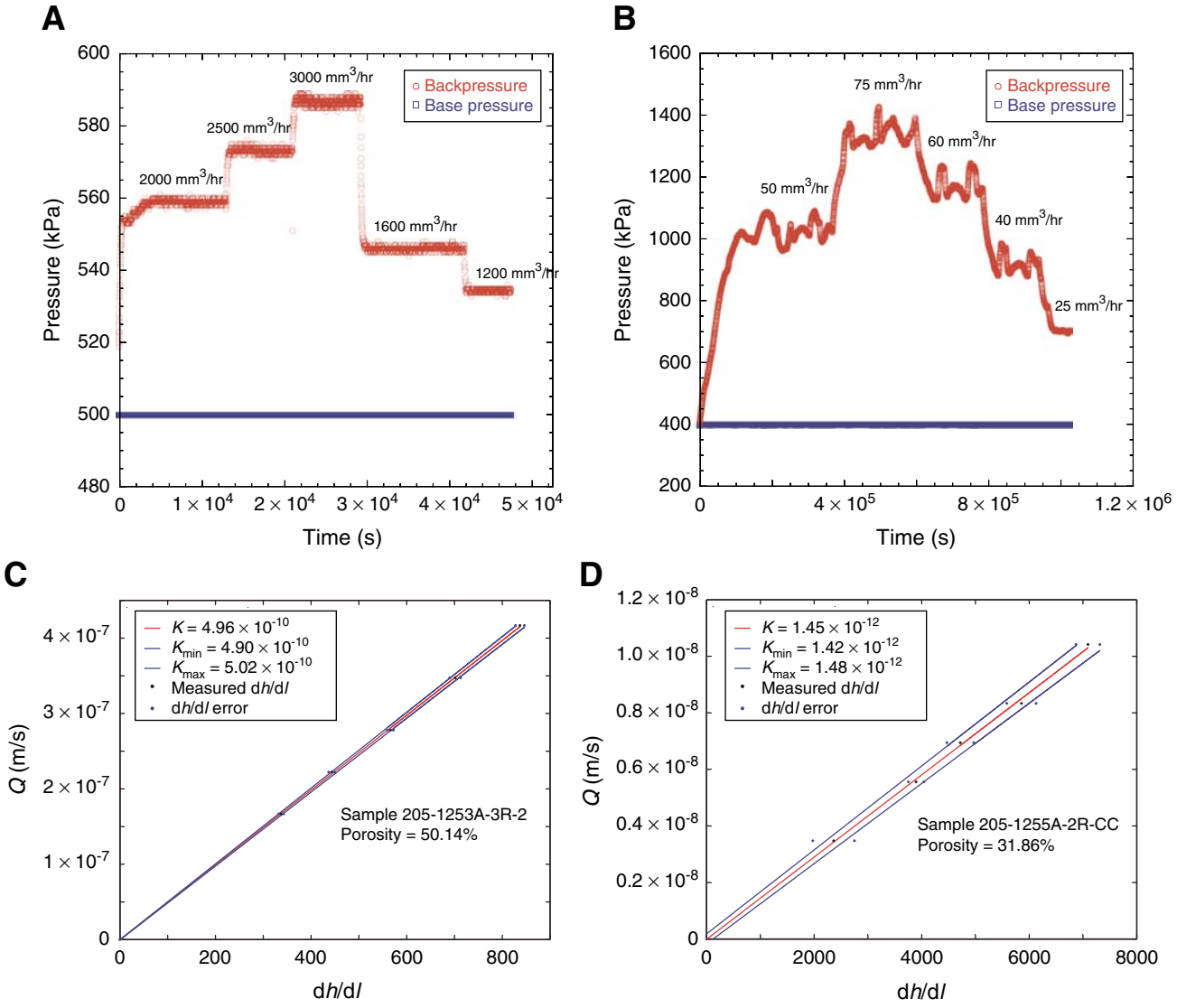

Figure F5. Leg 205 and 170 hemipelagic permeabilities. **A.** C_v-calculated and flow-through-determined permeabilities from Leg 205. **B.** All hemipelagic permeability data from Legs 205 and 170 (Saffer et al., 2000) with calculated relationship between porosity and permeability based on all available data. Equations for individual samples are presented in Table T5, p. 17.

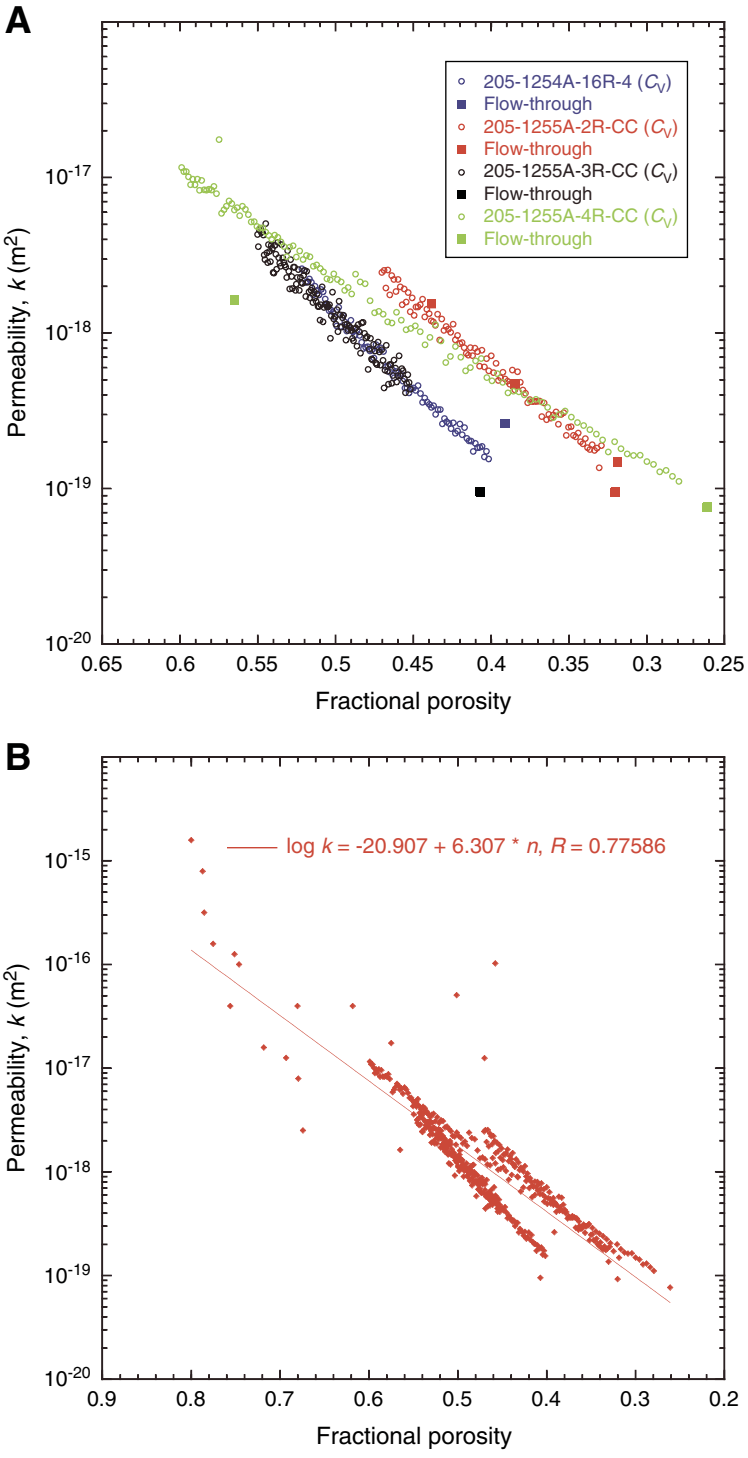

Figure F6. Flow-through permeability determinations for pelagic carbonate samples from Leg 205 (colored points, this study) and Leg 170 (Saffer et al., 2000).

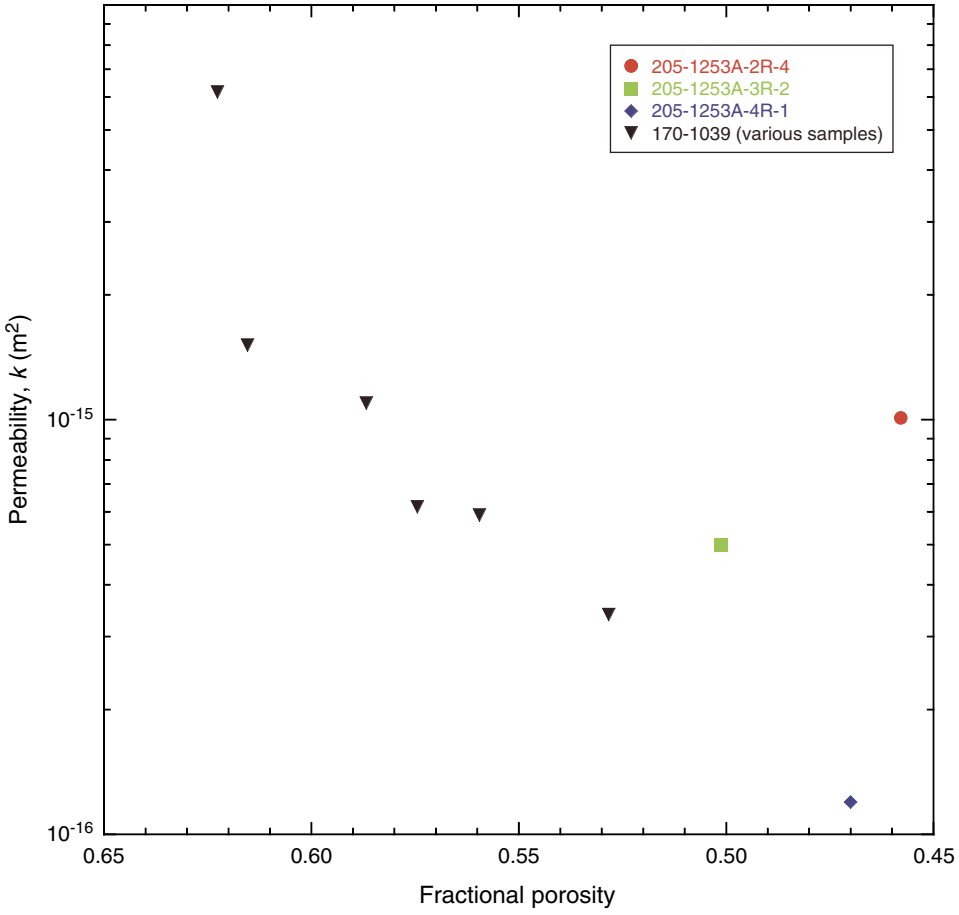

Table T1. Leg 205 sample locations.

Core, section, interval (cm)	Depth (mbsf)	Volume (cm^3)
205-1253A-		
2R-4, 43–60	380.07	599
3R-2, 13–24	386.83	388
4R-1, 1–12	394.91	388
205-1254A-		
16R- 4, 10–30	366.74	705
205-1255A-		
2R-CC, 0–8	134.89	282
3R-CC, 0–12	146.48	423
4R-CC, 0–8	152.38	282

Table T2. Consolidation properties, P_c' values, and in situ porosity and permeability estimates.

Core, section, interval (cm)	Elastic slope	C_c	P_c' (kPa)	In situ fractional porosity	In situ k (m/s)
205-1253A-					
2R-4, 43–60	0.097	1.225	2650	0.644	NA
3R-2, 13–24	0.102	1.322	1100	0.708	NA
4R-1, 1–12	0.158	1.427	3220	0.649	NA
205-1254A-					
16R-4, 10–30	0.042	0.567	730	0.569	5.90E–18
205-1255A-					
2R-CC, 0–8	0.007	0.504	1460	0.484	2.58E–18
3R-CC, 0–12	0.018	0.542	560	0.567	5.60E–18
4R-CC, 0–8	0.062	0.826	855	0.569	6.26E–18

Note: C_c = slope of virgin consolidation curve, P_c' = maximum preconsolidation stress, k = permeability.

Table T3. Equations for permeabilities calculated from C_v.

Core, section, interval (cm)	k_0	Slope
205-1254A-		
16R-4, 10–30	–22.723	9.711
205-1255A-		
2R-CC, 0–8	–21.473	8.157
3R-CC, 0–12	–22.733	9.699
4R-CC, 0–8	–20.77	6.298
Average*	–20.907	6.307

Notes: Values for predicted evolution of permeability and porosity, $\log(k) = k_0 + C_{cslope} \times n$. k = permeability, k_0 = fitted y-intercept, C_{cslope} = slope of the virgin consolidation curve, n = porosity. * = includes Saffer et al., 2000.

Table T4. Flow-through permeability test data.

Core, section, interval (cm)	Fractional porosity	Q (m^3/s)	dP (kPa)	dl (m)
205-1253A-				
2R-4, 43–60	0.459	6.94E–11	4 ± 0.433	0.0119419
	0.459	6.94E–10	40 ± 0.884	0.0119353
	0.458	5.56E–10	33 ± 0.734	0.0119254
	0.457	4.44E–10	26 ± 0.813	0.0119083
	0.456	3.33E–10	20 ± 0.793	0.0118878
3R-2, 13–24	0.503	5.56E–10	59 ± 0.669	0.0106253
	0.502	6.94E–10	73 ± 1.194	0.0106061
	0.501	8.33E–10	87 ± 0.961	0.0105931
	0.501	4.44E–10	46 ± 0.657	0.0105803
	0.500	3.33E–10	35 ± 0.533	0.0105713
4R-1, 1–12	0.472	5.56E–10	260 ± 3.461	0.0117188
	0.470	4.44E–10	211 ± 2.37	0.0116835
	0.470	3.33E–10	159 ± 1.685	0.0116739
	0.469	2.50E–10	120 ± 1.255	0.0116623
	0.469	1.25E–10	61 ± 1.142	0.0116562
205-1255A-				
16R-4, 10–30	0.392	1.39E–11	256 ± 22.205	0.013226
	0.391	2.08E–11	489 ± 37.471	0.0132064
	0.391	1.67E–11	443 ± 4.184	0.0132031
	0.391	1.11E–11	339 ± 15.489	0.013201
	0.391	6.94E–12	202 ± 3.774	0.0132
205-1255A-				
2R-CC, 0–8	0.317	1.39E–11	1065 ± 19.191	0.0139477
	0.322	1.11E–11	791 ± 46.222	0.014033
	0.322	6.94E–12	492 ± 37.413	0.014033
	0.322	9.17E–12	670 ± 36.687	0.0140336
	0.499	5.56E–10	10 ± 0.764	0.0183185
	0.499	8.33E–10	16 ± 1.744	0.0183185
	0.474	1.39E–11	13 ± 0.469	0.017465
	0.474	2.78E–11	29 ± 1.284	0.0174635
	0.474	4.17E–11	46 ± 0.504	0.017462
	0.439	1.39E–11	68 ± 3.163	0.016356
	0.438	2.78E–11	149 ± 5.830	0.01635
	0.438	2.08E–11	113 ± 5.201	0.01634
	0.438	6.94E–12	39 ± 3.368	0.01635
	0.386	1.39E–11	202 ± 8.277	0.0149486
	0.385	2.08E–11	311 ± 1.427	0.0149347
	0.385	2.78E–11	431 ± 18.947	0.0149235
	0.384	1.67E–11	332 ± 10.394	0.0149162
	0.384	6.94E–12	110 ± 5.008	0.014914
	0.320	1.39E–11	625 ± 33.214	0.0135007
	0.319	2.08E–11	938 ± 29.211	0.0134786
	0.318	1.67E–11	774 ± 35.999	0.0134723
	0.318	1.11E–11	515 ± 19.037	0.013469
	0.318	6.94E–12	312 ± 51.116	0.0134599
3R-CC, 0–12	0.407	6.94E–12	479 ± 6.034	0.0131541
	0.407	4.17E–12	290 ± 0.676	0.0131522
	0.407	5.56E–12	384 ± 9.251	0.0131519
4R-CC, 0–8	0.262	6.94E–12	454 ± 4.758	0.0101688
	0.261	5.56E–12	382 ± 8.071	0.0101535
	0.649	2.78E–11	27 ± 0.553	0.01899
	0.649	2.08E–11	21 ± 0.738	0.01899
	0.649	1.39E–11	15 ± 0.542	0.01899
	0.649	8.33E–12	9 ± 0.080	0.01899
	0.649	1.67E–11	17 ± 0.500	0.01899
	0.645	2.78E–11	31 ± 0.583	0.018774
	0.645	3.47E–11	39 ± 0.503	0.018774
	0.645	4.17E–11	46 ± 0.392	0.018774
	0.645	2.08E–11	23 ± 0.496	0.018774
	0.645	1.39E–11	16 ± 0.429	0.018774
	0.565	2.78E–11	129 ± 2.540	0.015336
	0.565	3.47E–11	165 ± 1.001	0.015336
	0.565	1.39E–11	66 ± 1.121	0.015336

Note: Q = flux into top of sample, dP = equilibrium pressure difference across sample, dl = length of most direct flow path (equal to height of sample).

Table T5. Flow-through permeability results and error.

Core, section, interval (cm)	Fractional porosity	k (m/s)	k_{min} (m/s)	k_{max} (m/s)
205-1253A-				
2R-4, 43–60	0.458	1.03E–16	1.01E–16	1.05E–16
3R-2, 13–24	0.501	5.068E–17	5.006E–17	5.132E–17
4R-1, 1–12	0.470	1.252E–17	1.237E–17	1.267E–17
205-1254A-				
16R-4, 10–30	0.391	2.624E–19	2.521E–19	2.712E–19
205-1255A-				
2R-CC, 0–8	0.320	9.254E–20	9.04E–20	9.448E–20
2R-CC, 0–8	0.499	4.81E–16	4.35E–16	5.38E–16
2R-CC, 0–8	0.474	7.862E–18	7.756E–18	7.963E–18
2R-CC, 0–8	0.438	1.524E–18	1.47E–18	1.582E–18
2R-CC, 0–8	0.385	4.566E–19	4.416E–19	5.026E–19
2R-CC, 0–8	0.319	1.485E–19	1.449E–19	1.516E–19
3R-CC, 0–12	0.407	9.548E–20	9.40E–07	9.699E–20
4R-CC, 0–8	0.261	7.661E–20	7.552E–20	7.773E–20
4R-CC, 0–8	0.649	9.758E–18	9.496E–18	1.003E–17
4R-CC, 0–8	0.645	8.495E–18	8.421E–18	8.569E–18
4R-CC, 0–8	0.565	1.629E–18	1.614E–18	1.644E–18

Note: k = least-squares (LS) fit to flow-through data, k_{min}/k_{max} = LS fit to flow-through data ± equilibrium pressure error.

Table T6. C_V, M_V, and resulting k values. (See table notes. Continued on next six pages.)

Core, section, interval (cm)	Axial displacement (mm)	C_v (m^2/s)	M_v (Pa^{-1})	k (m/s)
205-1254A-				
16R-4, 10–30	3.211	8.50E–08	3.04E–08	2.59E–18
	3.256	7.68E–08	3.27E–08	2.513E–18
	3.295	7.61E–08	2.77E–08	2.111E–18
	3.336	8.10E–08	2.64E–08	2.14E–18
	3.38	7.59E–08	2.93E–08	2.224E–18
	3.423	7.31E–08	2.90E–08	2.121E–18
	3.461	6.96E–08	2.52E–08	1.758E–18
	3.504	6.73E–08	2.97E–08	1.998E–18
	3.548	6.52E–08	2.87E–08	1.87E–18
	3.589	6.43E–08	2.73E–08	1.757E–18
	3.636	6.24E–08	3.05E–08	1.905E–18
	3.682	6.35E–08	2.89E–08	1.839E–18
	3.725	6.05E–08	2.73E–08	1.654E–18
	3.765	6.01E–08	2.52E–08	1.514E–18
	3.805	5.83E–08	2.38E–08	1.392E–18
	3.846	5.60E–08	2.50E–08	1.405E–18
	3.886	5.41E–08	2.51E–08	1.362E–18
	3.925	5.11E–08	2.46E–08	1.258E–18
	3.959	5.58E–08	1.98E–08	1.109E–18
	4.005	5.53E–08	2.64E–08	1.463E–18
	4.042	5.44E–08	2.02E–08	1.102E–18
	4.086	5.08E–08	2.56E–08	1.303E–18
	4.127	5.24E–08	2.24E–08	1.175E–18
	4.165	4.81E–08	2.14E–08	1.031E–18
	4.205	4.89E–08	2.17E–08	1.061E–18
	4.252	4.71E–08	2.56E–08	1.206E–18
	4.293	4.70E–08	2.16E–08	1.019E–18
	4.333	4.66E–08	2.07E–08	9.671E–19
	4.377	4.53E–08	2.31E–08	1.047E–18
	4.419	4.40E–08	2.19E–08	9.637E–19
	4.459	4.31E–08	2.02E–08	8.707E–19
	4.496	4.14E–08	1.92E–08	7.939E–19
	4.535	4.19E–08	1.93E–08	8.091E–19
	4.576	4.01E–08	2.03E–08	8.162E–19
	4.614	4.14E–08	1.86E–08	7.685E–19
	4.655	3.94E–08	1.97E–08	7.765E–19
	4.691	3.94E–08	1.75E–08	6.908E–19
	4.738	3.88E–08	2.17E–08	8.421E–19
	4.783	3.82E–08	2.04E–08	7.801E–19
	4.829	3.78E–08	2.12E–08	8.021E–19
	4.874	3.78E–08	2.01E–08	7.607E–19
	4.912	3.76E–08	1.61E–08	6.069E–19
	4.951	3.54E–08	1.74E–08	6.162E–19
	4.987	3.69E–08	1.52E–08	5.609E–19
	5.026	3.62E–08	1.61E–08	5.83E–19
	5.061	3.40E–08	1.51E–08	5.146E–19
	5.101	3.38E–08	1.67E–08	5.651E–19
	5.141	3.35E–08	1.65E–08	5.553E–19
	5.182	3.22E–08	1.70E–08	5.476E–19
	5.22	3.25E–08	1.51E–08	4.91E–19
	5.255	3.27E–08	1.35E–08	4.417E–19
	5.291	3.11E–08	1.42E–08	4.429E–19
	5.325	3.17E–08	1.30E–08	4.121E–19
	5.362	3.25E–08	1.35E–08	4.378E–19
	5.401	3.06E–08	1.45E–08	4.436E–19
	5.439	3.04E–08	1.41E–08	4.277E–19
	5.482	2.92E–08	1.57E–08	4.588E–19
	5.52	2.94E–08	1.39E–08	4.076E–19
	5.555	2.80E–08	1.28E–08	3.577E–19
	5.593	2.92E–08	1.30E–08	3.815E–19
	5.629	2.93E–08	1.23E–08	3.601E–19
	5.665	2.90E–08	1.20E–08	3.475E–19
	5.7	2.86E–08	1.16E–08	3.33E–19
	5.737	2.80E–08	1.21E–08	3.404E–19
	5.771	2.72E–08	1.10E–08	3.001E–19
	5.808	2.69E–08	1.20E–08	3.222E–19

Table T6 (continued).

Core, section, interval (cm)	Axial displacement (mm)	C_v (m^2/s)	M_v (Pa^{-1})	k (m/s)
	5.846	2.55E–08	1.26E–08	3.22E–19
	5.878	2.61E–08	9.97E–09	2.605E–19
	5.913	2.66E–08	1.06E–08	2.817E–19
	5.947	2.54E–08	1.06E–08	2.692E–19
	5.981	2.63E–08	9.95E–09	2.62E–19
	6.014	2.44E–08	9.94E–09	2.428E–19
	6.05	2.48E–08	1.06E–08	2.642E–19
	6.082	2.38E–08	9.51E–09	2.267E–19
	6.116	2.37E–08	9.86E–09	2.345E–19
	6.154	2.38E–08	1.09E–08	2.603E–19
	6.188	2.27E–08	9.75E–09	2.222E–19
	6.225	2.47E–08	9.96E–09	2.464E–19
	6.258	2.29E–08	9.14E–09	2.102E–19
	6.291	2.20E–08	9.19E–09	2.029E–19
	6.324	2.29E–08	8.78E–09	2.017E–19
	6.353	2.22E–08	7.79E–09	1.73E–19
	6.386	2.26E–08	8.63E–09	1.954E–19
	6.418	2.14E–08	8.52E–09	1.83E–19
	6.451	2.19E–08	8.38E–09	1.841E–19
	6.485	2.16E–08	8.63E–09	1.865E–19
	6.515	2.06E–08	7.71E–09	1.595E–19
	6.548	2.13E–08	8.12E–09	1.735E–19
	6.578	2.04E–08	7.57E–09	1.549E–19
205-1255A-				
2R-CC, 0–8	2.052	8.15E–08	3.00E–08	2.452E–18
	2.099	7.81E–08	3.23E–08	2.528E–18
	2.136	7.71E–08	2.52E–08	1.946E–18
	2.184	7.65E–08	3.32E–08	2.543E–18
	2.219	7.24E–08	2.42E–08	1.757E–18
	2.267	7.67E–08	3.05E–08	2.344E–18
	2.313	7.85E–08	2.81E–08	2.209E–18
	2.353	7.15E–08	2.58E–08	1.846E–18
	2.402	7.32E–08	3.01E–08	2.207E–18
	2.446	6.63E–08	2.98E–08	1.977E–18
	2.481	6.58E–08	2.30E–08	1.515E–18
	2.527	7.11E–08	2.69E–08	1.918E–18
	2.564	6.68E–08	2.35E–08	1.575E–18
	2.61	6.72E–08	2.70E–08	1.819E–18
	2.645	6.28E–08	2.18E–08	1.371E–18
	2.689	6.37E–08	2.63E–08	1.676E–18
	2.725	6.23E–08	2.08E–08	1.298E–18
	2.766	5.94E–08	2.47E–08	1.47E–18
	2.807	5.95E–08	2.46E–08	1.466E–18
	2.851	5.93E–08	2.55E–08	1.517E–18
	2.9	5.65E–08	2.91E–08	1.648E–18
	2.939	5.62E–08	2.25E–08	1.267E–18
	2.984	5.55E–08	2.56E–08	1.421E–18
	3.027	5.65E–08	2.35E–08	1.329E–18
	3.067	5.36E–08	2.24E–08	1.201E–18
	3.107	4.95E–08	2.37E–08	1.175E–18
	3.146	5.22E–08	2.15E–08	1.123E–18
	3.192	5.37E–08	2.45E–08	1.319E–18
	3.224	4.98E–08	1.81E–08	9.024E–19
	3.27	4.95E–08	2.47E–08	1.225E–18
	3.31	4.77E–08	2.17E–08	1.038E–18
	3.352	5.04E–08	2.17E–08	1.096E–18
	3.394	4.80E–08	2.20E–08	1.058E–18
	3.436	4.71E–08	2.15E–08	1.013E–18
	3.484	4.65E–08	2.45E–08	1.141E–18
	3.522	4.54E–08	1.99E–08	9.043E–19
	3.564	4.62E–08	2.09E–08	9.645E–19
	3.603	4.38E–08	1.95E–08	8.548E–19
	3.644	4.32E–08	2.01E–08	8.688E–19
	3.682	4.33E–08	1.86E–08	8.046E–19
	3.718	4.27E–08	1.73E–08	7.391E–19
	3.754	4.25E–08	1.69E–08	7.195E–19
	3.795	4.08E–08	1.97E–08	8.055E–19
	3.833	4.23E–08	1.69E–08	7.149E–19

Table T6 (continued).

Core, section, interval (cm)	Axial displacement (mm)	C_v (m^2/s)	M_v (Pa^{-1})	k (m/s)
	3.876	4.10E–08	1.95E–08	7.996E–19
	3.918	3.92E–08	1.93E–08	7.593E–19
	3.953	3.99E–08	1.53E–08	6.12E–19
	3.998	3.95E–08	1.96E–08	7.763E–19
	4.035	3.71E–08	1.63E–08	6.043E–19
	4.077	3.85E–08	1.77E–08	6.825E–19
	4.114	3.54E–08	1.61E–08	5.713E–19
	4.159	3.86E–08	1.84E–08	7.129E–19
	4.196	3.86E–08	1.44E–08	5.567E–19
	4.239	3.67E–08	1.74E–08	6.393E–19
	4.273	3.63E–08	1.36E–08	4.948E–19
	4.31	3.50E–08	1.47E–08	5.162E–19
	4.351	3.43E–08	1.63E–08	5.593E–19
	4.389	3.58E–08	1.41E–08	5.061E–19
	4.427	3.36E–08	1.45E–08	4.89E–19
	4.464	3.38E–08	1.38E–08	4.691E–19
	4.511	3.36E–08	1.72E–08	5.782E–19
	4.547	3.25E–08	1.32E–08	4.308E–19
	4.595	3.21E–08	1.75E–08	5.628E–19
	4.638	3.18E–08	1.52E–08	4.833E–19
	4.677	3.05E–08	1.41E–08	4.305E–19
	4.715	2.99E–08	1.37E–08	4.102E–19
	4.749	3.03E–08	1.17E–08	3.558E–19
	4.785	3.06E–08	1.22E–08	3.73E–19
	4.821	2.98E–08	1.21E–08	3.616E–19
	4.858	2.99E–08	1.21E–08	3.642E–19
	4.896	2.85E–08	1.28E–08	3.634E–19
	4.936	2.69E–08	1.36E–08	3.653E–19
	4.968	2.81E–08	1.03E–08	2.905E–19
	5.008	2.79E–08	1.27E–08	3.55E–19
	5.04	2.84E–08	9.75E–09	2.773E–19
	5.075	2.77E–08	1.08E–08	3.001E–19
	5.109	2.75E–08	1.03E–08	2.834E–19
	5.146	2.70E–08	1.10E–08	2.974E–19
	5.185	2.64E–08	1.18E–08	3.112E–19
	5.219	2.56E–08	1.01E–08	2.588E–19
	5.259	2.58E–08	1.16E–08	2.993E–19
	5.301	2.48E–08	1.24E–08	3.073E–19
	5.332	2.46E–08	8.93E–09	2.198E–19
	5.367	2.50E–08	9.89E–09	2.476E–19
	5.404	2.41E–08	1.04E–08	2.502E–19
	5.437	2.41E–08	9.11E–09	2.199E–19
	5.47	2.43E–08	8.84E–09	2.151E–19
	5.506	2.23E–08	1.02E–08	2.272E–19
	5.538	2.29E–08	8.74E–09	2.004E–19
	5.57	2.31E–08	8.38E–09	1.938E–19
	5.605	2.24E–08	9.29E–09	2.088E–19
	5.637	2.13E–08	8.58E–09	1.835E–19
	5.668	2.29E–08	7.77E–09	1.783E–19
	5.702	2.23E–08	8.55E–09	1.906E–19
	5.734	2.16E–08	8.13E–09	1.761E–19
	5.768	2.15E–08	8.46E–09	1.824E–19
	5.794	2.07E–08	6.53E–09	1.356E–19
	5.831	2.05E–08	9.24E–09	1.894E–19
205-1255A-				
3R–CC, 0–12	2.677	5.74E–08	7.48E–08	4.305E–18
	2.697	5.74E–08	6.24E–08	3.594E–18
	2.721	5.68E–08	8.13E–08	4.629E–18
	2.747	5.89E–08	8.01E–08	4.727E–18
	2.769	5.57E–08	7.91E–08	4.417E–18
	2.794	4.96E–08	8.97E–08	4.457E–18
	2.819	5.17E–08	8.24E–08	4.266E–18
	2.837	5.90E–08	5.36E–08	3.17E–18
	2.855	5.50E–08	5.37E–08	2.96E–18
	2.882	4.53E–08	1.11E–07	5.05E–18
	2.904	4.95E–08	6.59E–08	3.266E–18
	2.922	5.16E–08	5.47E–08	2.832E–18
	2.946	5.33E–08	6.94E–08	3.703E–18

Table T6 (continued).

Core, section, interval (cm)	Axial displacement (mm)	C_v (m^2/s)	M_v (Pa^{-1})	k (m/s)
	2.97	5.69E–08	5.88E–08	3.351E–18
	2.988	5.02E–08	5.71E–08	2.87E–18
	3.012	5.02E–08	7.31E–08	3.672E–18
	3.035	4.78E–08	7.26E–08	3.475E–18
	3.053	5.79E–08	4.22E–08	2.449E–18
	3.071	5.56E–08	4.36E–08	2.427E–18
	3.095	4.21E–08	8.68E–08	3.661E–18
	3.118	5.38E–08	5.97E–08	3.213E–18
	3.137	5.53E–08	4.64E–08	2.571E–18
	3.164	4.22E–08	9.08E–08	3.833E–18
	3.187	5.12E–08	5.95E–08	3.052E–18
	3.208	4.71E–08	5.95E–08	2.809E–18
	3.229	5.48E–08	4.91E–08	2.692E–18
	3.257	4.85E–08	7.61E–08	3.701E–18
	3.28	4.22E–08	7.19E–08	3.042E–18
	3.305	5.07E–08	5.63E–08	2.857E–18
	3.329	4.49E–08	6.08E–08	2.735E–18
	3.349	5.10E–08	5.21E–08	2.661E–18
	3.369	5.09E–08	4.45E–08	2.27E–18
	3.395	4.88E–08	6.91E–08	3.383E–18
	3.419	4.72E–08	5.27E–08	2.491E–18
	3.435	4.50E–08	4.26E–08	1.921E–18
	3.461	4.85E–08	6.09E–08	2.958E–18
	3.482	4.94E–08	4.66E–08	2.309E–18
	3.5	4.27E–08	4.52E–08	1.935E–18
	3.525	4.06E–08	6.52E–08	2.651E–18
	3.55	4.78E–08	5.54E–08	2.652E–18
	3.568	4.88E–08	3.85E–08	1.885E–18
	3.587	5.28E–08	3.89E–08	2.056E–18
	3.61	4.05E–08	5.59E–08	2.27E–18
	3.635	4.40E–08	5.80E–08	2.557E–18
	3.653	4.76E–08	3.94E–08	1.88E–18
	3.677	4.29E–08	5.31E–08	2.278E–18
	3.699	4.23E–08	4.97E–08	2.109E–18
	3.721	4.32E–08	4.80E–08	2.077E–18
	3.747	4.72E–08	4.96E–08	2.344E–18
	3.772	4.11E–08	6.15E–08	2.531E–18
	3.792	4.24E–08	4.05E–08	1.721E–18
	3.819	4.32E–08	5.74E–08	2.487E–18
	3.843	4.17E–08	5.08E–08	2.118E–18
	3.864	4.29E–08	4.29E–08	1.842E–18
	3.884	3.89E–08	4.31E–08	1.678E–18
	3.907	4.04E–08	4.64E–08	1.881E–18
	3.929	4.40E–08	4.41E–08	1.946E–18
	3.949	3.81E–08	4.12E–08	1.572E–18
	3.971	3.99E–08	4.60E–08	1.837E–18
	3.993	4.16E–08	4.04E–08	1.68E–18
	4.014	3.99E–08	3.99E–08	1.597E–18
	4.037	3.81E–08	4.67E–08	1.784E–18
	4.057	3.99E–08	3.70E–08	1.478E–18
	4.077	3.54E–08	4.16E–08	1.476E–18
	4.093	4.15E–08	2.91E–08	1.21E–18
	4.115	4.21E–08	3.61E–08	1.522E–18
	4.141	4.12E–08	4.80E–08	1.982E–18
	4.158	3.45E–08	3.41E–08	1.179E–18
	4.179	3.60E–08	4.03E–08	1.457E–18
	4.203	3.83E–08	3.99E–08	1.532E–18
	4.225	3.99E–08	3.85E–08	1.539E–18
	4.247	3.50E–08	4.20E–08	1.473E–18
	4.27	3.69E–08	4.00E–08	1.481E–18
	4.293	4.35E–08	3.50E–08	1.522E–18
	4.308	3.37E–08	2.74E–08	9.234E–19
	4.329	3.29E–08	3.91E–08	1.287E–18
	4.358	3.92E–08	4.66E–08	1.831E–18
	4.379	3.31E–08	3.71E–08	1.232E–18
	4.4	3.58E–08	3.56E–08	1.278E–18
	4.42	3.09E–08	3.67E–08	1.137E–18
	4.444	3.63E–08	3.87E–08	1.405E–18

Table T6 (continued).

Core, section, interval (cm)	Axial displacement (mm)	C_v (m^2/s)	M_v (Pa^{-1})	k (m/s)
	4.462	3.67E–08	2.76E–08	1.015E–18
	4.489	3.65E–08	4.38E–08	1.60E–18
	4.512	3.52E–08	3.71E–08	1.307E–18
	4.532	3.46E–08	3.15E–08	1.092E–18
	4.555	3.61E–08	3.45E–08	1.246E–18
	4.579	3.50E–08	3.71E–08	1.301E–18
	4.601	3.29E–08	3.43E–08	1.131E–18
	4.618	3.43E–08	2.62E–08	9.009E–19
	4.641	3.27E–08	3.50E–08	1.144E–18
	4.661	3.47E–08	2.98E–08	1.036E–18
	4.683	3.11E–08	3.55E–08	1.107E–18
	4.705	3.27E–08	3.31E–08	1.082E–18
	4.727	3.77E–08	2.75E–08	1.039E–18
	4.746	2.88E–08	3.20E–08	9.227E–19
	4.766	3.18E–08	2.80E–08	8.911E–19
	4.789	3.15E–08	3.35E–08	1.057E–18
	4.812	3.38E–08	3.21E–08	1.085E–18
	4.831	3.25E–08	2.52E–08	8.217E–19
	4.857	3.12E–08	3.63E–08	1.134E–18
	4.88	3.00E–08	3.41E–08	1.023E–18
	4.898	3.08E–08	2.40E–08	7.414E–19
	4.924	3.05E–08	3.80E–08	1.163E–18
	4.952	2.89E–08	4.05E–08	1.172E–18
	4.977	2.85E–08	3.49E–08	9.945E–19
	5	3.29E–08	2.82E–08	9.289E–19
	5.024	2.95E–08	3.22E–08	9.492E–19
	5.039	2.90E–08	2.01E–08	5.828E–19
	5.06	2.72E–08	2.89E–08	7.874E–19
	5.084	2.95E–08	3.12E–08	9.23E–19
	5.102	2.82E–08	2.41E–08	6.799E–19
	5.121	2.62E–08	2.56E–08	6.735E–19
	5.144	2.67E–08	3.17E–08	8.453E–19
	5.165	2.77E–08	2.76E–08	7.657E–19
	5.183	2.71E–08	2.36E–08	6.413E–19
	5.201	2.64E–08	2.37E–08	6.263E–19
	5.226	2.71E–08	3.22E–08	8.747E–19
	5.248	2.91E–08	2.60E–08	7.56E–19
	5.267	2.44E–08	2.54E–08	6.219E–19
	5.292	2.52E–08	3.09E–08	7.81E–19
	5.313	2.34E–08	2.85E–08	6.681E–19
	5.327	2.55E–08	1.74E–08	4.426E–19
	5.346	2.67E–08	2.16E–08	5.768E–19
	5.372	2.66E–08	3.13E–08	8.352E–19
	5.391	2.67E–08	2.12E–08	5.681E–19
	5.407	2.53E–08	1.85E–08	4.693E–19
	5.428	2.66E–08	2.36E–08	6.277E–19
	5.45	2.46E–08	2.53E–08	6.224E–19
	5.467	2.61E–08	1.82E–08	4.747E–19
	5.485	2.43E–08	2.19E–08	5.33E–19
	5.509	2.47E–08	2.70E–08	6.695E–19
	5.531	2.51E–08	2.36E–08	5.943E–19
	5.549	2.35E–08	2.06E–08	4.842E–19
	5.569	2.49E–08	2.13E–08	5.316E–19
	5.596	2.63E–08	2.71E–08	7.133E–19
	5.616	2.27E–08	2.34E–08	5.306E–19
	5.639	2.29E–08	2.57E–08	5.899E–19
	5.662	2.56E–08	2.23E–08	5.727E–19
	5.682	2.28E–08	2.21E–08	5.061E–19
	5.699	2.34E–08	1.76E–08	4.132E–19
	5.719	2.19E–08	2.16E–08	4.752E–19
	5.742	2.34E–08	2.31E–08	5.398E–19
	5.762	2.14E–08	2.24E–08	4.796E–19
	5.781	2.33E–08	1.86E–08	4.353E–19
205-1255A-				
4R-CC, 0–8	1.312	9.10E–08	1.27E–07	1.158E–17
	1.379	1.00E–07	1.09E–07	1.088E–17
	1.448	9.25E–08	1.18E–07	1.09E–17
	1.514	1.07E–07	9.42E–08	1.006E–17

Table T6 (continued).

Core, section, interval (cm)	Axial displacement (mm)	C_v (m^2/s)	M_v (Pa^{-1})	k (m/s)
	1.575	1.08E–07	8.32E–08	8.977E–18
	1.64	1.14E–07	8.54E–08	9.749E–18
	1.705	1.13E–07	7.93E–08	8.949E–18
	1.773	1.19E–07	8.18E–08	9.764E–18
	1.828	1.36E–07	6.07E–08	8.257E–18
	1.897	1.20E–07	7.98E–08	9.559E–18
	1.962	1.10E–07	7.58E–08	8.339E–18
	2.03	1.18E–07	7.02E–08	8.282E–18
	2.098	1.13E–07	7.41E–08	8.415E–18
	2.167	9.45E–08	8.78E–08	8.308E–18
	2.235	4.53E–08	1.93E–07	8.759E–18
	2.302	2.77E–08	2.83E–07	7.857E–18
	2.37	1.17E–08	1.49E–06	1.751E–17
	2.438	1.57E–08	3.73E–07	5.876E–18
	2.502	1.16E–07	5.34E–08	6.209E–18
	2.566	1.63E–07	4.02E–08	6.542E–18
	2.638	1.50E–07	4.70E–08	7.057E–18
	2.708	1.19E–07	5.69E–08	6.787E–18
	2.772	8.98E–08	6.87E–08	6.181E–18
	2.84	8.31E–08	7.68E–08	6.399E–18
	2.905	6.87E–08	8.26E–08	5.681E–18
	2.977	5.71E–08	1.14E–07	6.533E–18
	3.053	6.03E–08	1.03E–07	6.244E–18
	3.123	5.66E–08	1.02E–07	5.756E–18
	3.194	5.19E–08	9.96E–08	5.18E–18
	3.263	4.68E–08	1.11E–07	5.20E–18
	3.331	5.19E–08	9.30E–08	4.837E–18
	3.399	4.96E–08	9.48E–08	4.706E–18
	3.469	4.92E–08	9.64E–08	4.754E–18
	3.538	4.67E–08	9.50E–08	4.448E–18
	3.608	5.05E–08	8.38E–08	4.243E–18
	3.674	4.85E–08	8.24E–08	4.007E–18
	3.743	4.72E–08	9.00E–08	4.256E–18
	3.813	4.88E–08	8.43E–08	4.118E–18
	3.886	4.20E–08	9.15E–08	3.854E–18
	3.95	4.48E–08	8.02E–08	3.604E–18
	4.009	4.07E–08	7.62E–08	3.104E–18
	4.081	3.89E–08	9.13E–08	3.555E–18
	4.155	3.97E–08	9.15E–08	3.644E–18
	4.22	3.82E–08	8.05E–08	3.079E–18
	4.293	3.53E–08	9.55E–08	3.371E–18
	4.363	3.49E–08	8.49E–08	2.967E–18
	4.434	3.75E–08	8.38E–08	3.153E–18
	4.508	3.55E–08	8.70E–08	3.091E–18
	4.575	3.03E–08	8.87E–08	2.689E–18
	4.647	3.55E–08	7.71E–08	2.741E–18
	4.715	3.22E–08	8.04E–08	2.597E–18
	4.782	3.16E–08	7.82E–08	2.474E–18
	4.846	3.12E–08	7.13E–08	2.233E–18
	4.913	3.07E–08	7.15E–08	2.199E–18
	4.986	3.04E–08	7.89E–08	2.401E–18
	5.055	2.92E–08	7.54E–08	2.205E–18
	5.125	2.98E–08	7.16E–08	2.135E–18
	5.189	2.75E–08	6.84E–08	1.881E–18
	5.258	2.78E–08	7.03E–08	1.958E–18
	5.319	3.56E–08	4.99E–08	1.777E–18
	5.402	4.41E–08	5.42E–08	2.391E–18
	5.489	3.43E–08	6.21E–08	2.132E–18
	5.582	3.03E–08	6.82E–08	2.07E–18
	5.663	2.83E–08	5.68E–08	1.609E–18
	5.741	2.01E–08	6.70E–08	1.346E–18
	5.814	2.99E–08	4.59E–08	1.377E–18
	5.889	2.39E–08	5.52E–08	1.321E–18
	5.965	1.94E–08	6.07E–08	1.177E–18
	6.036	2.38E–08	4.87E–08	1.16E–18
	6.116	2.86E–08	4.75E–08	1.361E–18
	6.193	2.49E–08	4.84E–08	1.208E–18
	6.27	1.87E–08	5.62E–08	1.055E–18

Table T6 (continued).

Core, section, interval (cm)	Axial displacement (mm)	C_v (m^2/s)	M_v (Pa^{-1})	k (m/s)
	6.345	2.29E–08	4.67E–08	1.072E–18
	6.421	2.67E–08	4.17E–08	1.113E–18
	6.495	2.48E–08	4.11E–08	1.021E–18
	6.568	1.78E–08	4.72E–08	8.413E–19
	6.648	2.02E–08	4.63E–08	9.369E–19
	6.738	2.52E–08	4.49E–08	1.134E–18
	6.815	2.20E–08	4.04E–08	8.894E–19
	6.883	1.60E–08	4.02E–08	6.464E–19
	6.951	2.07E–08	3.40E–08	7.062E–19
	7.031	2.26E–08	3.61E–08	8.186E–19
	7.103	2.03E–08	3.43E–08	6.978E–19
	7.169	1.76E–08	3.24E–08	5.705E–19
	7.237	1.89E–08	3.17E–08	5.986E–19
	7.312	2.14E–08	3.09E–08	6.615E–19
	7.394	2.10E–08	3.25E–08	6.851E–19
	7.466	1.56E–08	3.31E–08	5.166E–19
	7.534	1.69E–08	2.91E–08	4.933E–19
	7.606	2.17E–08	2.51E–08	5.47E–19
	7.676	1.90E–08	2.52E–08	4.812E–19
	7.745	1.46E–08	2.81E–08	4.117E–19
	7.815	1.56E–08	2.71E–08	4.228E–19
	7.882	1.95E–08	2.14E–08	4.194E–19
	7.951	1.79E–08	2.23E–08	4.005E–19
	8.025	1.33E–08	2.76E–08	3.671E–19
	8.099	1.50E–08	2.49E–08	3.746E–19
	8.168	1.78E–08	2.01E–08	3.599E–19
	8.236	1.66E–08	2.00E–08	3.331E–19
	8.303	1.33E–08	2.15E–08	2.865E–19
	8.371	1.43E–08	2.09E–08	2.992E–19
	8.443	1.70E–08	1.85E–08	3.15E–19
	8.513	1.57E–08	1.83E–08	2.884E–19
	8.582	1.53E–08	1.74E–08	2.661E–19
	8.651	1.52E–08	1.67E–08	2.542E–19
	8.72	1.47E–08	1.62E–08	2.389E–19
	8.789	1.38E–08	1.62E–08	2.239E–19
	8.855	1.33E–08	1.54E–08	2.048E–19
	8.914	1.27E–08	1.35E–08	1.721E–19
	8.983	1.38E–08	1.45E–08	1.995E–19
	9.048	1.36E–08	1.32E–08	1.801E–19
	9.112	1.22E–08	1.36E–08	1.67E–19
	9.177	1.24E–08	1.31E–08	1.634E–19
	9.245	1.25E–08	1.31E–08	1.638E–19
	9.309	1.22E–08	1.22E–08	1.492E–19
	9.373	1.19E–08	1.19E–08	1.427E–19
	9.432	1.15E–08	1.11E–08	1.282E–19
	9.494	1.16E–08	1.12E–08	1.306E–19
	9.554	1.16E–08	1.04E–08	1.202E–19
	9.613	1.06E–08	1.04E–08	1.113E–19

Note: C_v = coefficient of consolidation, M_v = coefficient of volume compressibility, k = permeability.